Cell Reports, Volume *36*

Supplemental information

Systematic analysis of SARS-CoV-2 infection of an ACE2-negative human airway cell

Maritza Puray-Chavez, Kyle M. LaPak, Travis P. Schrank, Jennifer L. Elliott, Dhaval P. Bhatt, Megan J. Agajanian, Ria Jasuja, Dana Q. Lawson, Keanu Davis, Paul W. Rothlauf, Zhuoming Liu, Heejoon Jo, Nakyung Lee, Kasyap Tenneti, Jenna E. Eschbach, Christian Shema Mugisha, Emily M. Cousins, Erica W. Cloer, Hung R. Vuong, Laura A. VanBlargan, Adam L. Bailey, Pavlo Gilchuk, James E. Crowe Jr., Michael S. Diamond, D. Neil Hayes, Sean P.J. Whelan, Amjad Horani, Steven L. Brody, Dennis Goldfarb, M. Ben Major, and Sebla B. Kutluay

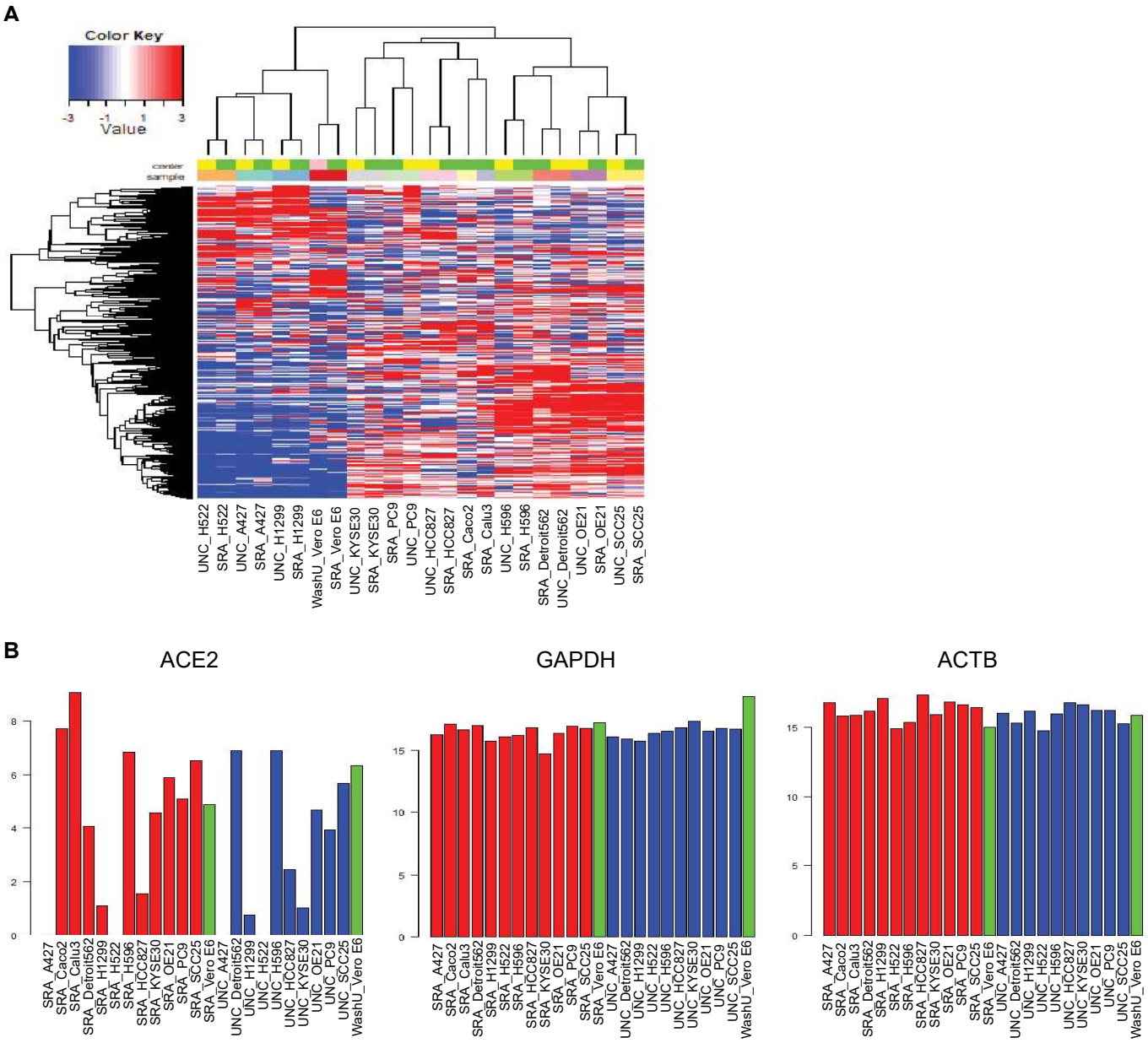
A
Color Key
-3
-1
1
3
Value
center
sample
UNC_H522
SRA_H522
UNC_A427
SRA_A427
UNC_H1299
SRA_H1299
WashU_Vero E6
SRA_Vero E6
UNC_KYSE30
SRA_KYSE30
SRA_PC9
UNC_PC9
UNC_HCC827
SRA_HCC827
SRA_Caco2
SRA_Calu3
UNC_H596
SRA_H596
SRA_Detroit562
UNC_Detroit562
UNC_OE21
SRA_OE21
UNC_SCC25
SRA_SCC25
B
ACE2
GAPDH
ACTB
SRA_A427
SRA_Caco2
SRA_Calu3
SRA_Detroit562
SRA_H1299
SRA_H522
SRA_H596
SRA_HCC827
SRA_KYSE30
SRA_OE21
SRA_PC9
SRA_SCC25
SRA_Vero E6
UNC_A427
UNC_Detroit562
UNC_H1299
UNC_H522
UNC_H596
UNC_HCC827
UNC_KYSE30
UNC_OE21
UNC_PC9
UNC_SCC25
WashU_Vero E6

Figure S1

Figure S1. Expression of *ACE2* across cell line models, related to Figure 1. A, Unsupervised hierarchical clustering of upper quartile-normalized RNA-seq reads. Normalized RNA-seq reads were aligned to the GRCh38 and Vervet-African green monkey genomes and quantified with Salmon (v1.3.0). As indicated, RNA-seq data were generated at UNC or Washington University or obtained from the Sequence Read Archive (SRA). **B,** Read counts for *ACE2*, *GAPDH* and *ACTB* across the indicated cell models.

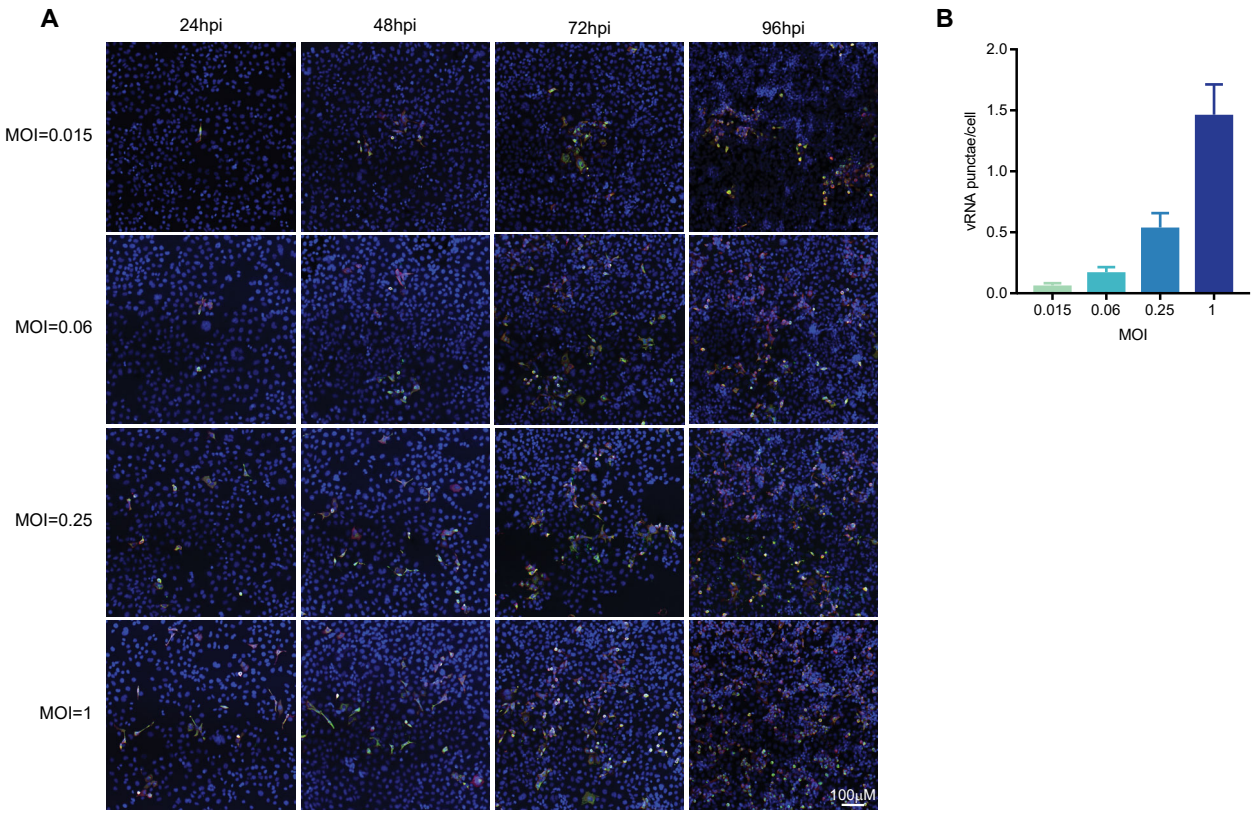
A
24hpi
48hpi
72hpi
96hpi
MOI=0.015
MOI=0.06
MOI=0.25
MOI=1
100μM
B
vRNA punctae/cell
2.0
1.5
1.0
0.5
0.0
0.015
0.06
0.25
1
MOI

Figure S2

Figure S2. Visualization of SARS-Cov-2 replication and spread in H522 cells, related to Figure 1. A, Representative images of H522 cells infected with SARS-CoV-2 at the indicated time points and MOIs. H522 cells were fixed and stained for SARS-CoV-2 RNA (green) by RNAScope reagents and Nucleocapsid (N) protein (red) and imaged by confocal microscopy (n=2). **B**, Quantification of vRNA puncta in H522 cells infected with variable MOIs of SARS-CoV-2. Greater than 150 cells per sample from 5 different fields were counted in a blinded manner from a representative experiment.

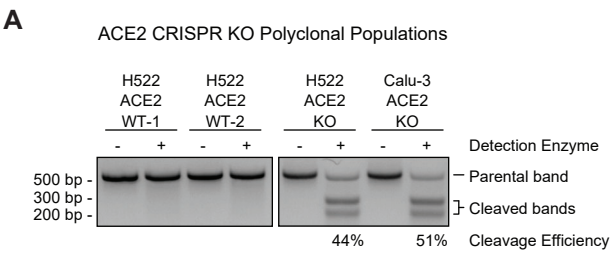
A
ACE2 CRISPR KO Polyclonal Populations
H522 ACE2 WT-1
H522 ACE2 WT-2
H522 ACE2 KO
Calu-3 ACE2 KO
- + - + - + - +
Detection Enzyme
500 bp -
300 bp -
200 bp -
Parental band
Cleaved bands
44%
51%
Cleavage Efficiency

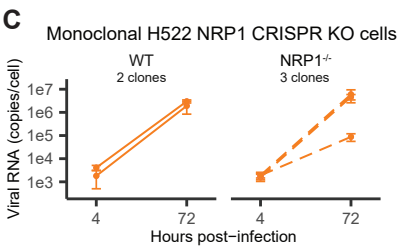
C
Monoclonal H522 NRP1 CRISPR KO cells
WT
2 clones
NRP1-/-
3 clones
Viral RNA (copies/cell)
1e7
1e6
1e5
1e4
1e3
4
72
4
72
Hours post−infection

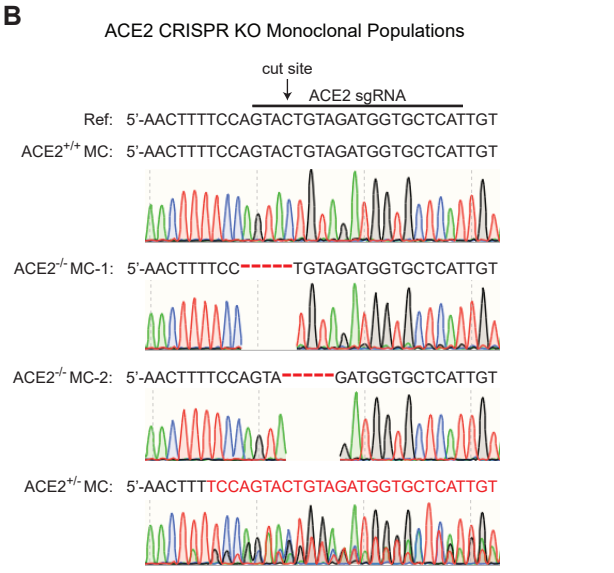
B
ACE2 CRISPR KO Monoclonal Populations
cut site
ACE2 sgRNA
Ref: 5'-AACTTTTCCAGTACTGTAGATGGTGCTCATTGT
ACE2+/+ MC: 5'-AACTTTTCCAGTACTGTAGATGGTGCTCATTGT
ACE2-/- MC-1: 5'-AACTTTTCC-----TGTAGATGGTGCTCATTGT
ACE2-/- MC-2: 5'-AACTTTTCCAGTA-----GATGGTGCTCATTGT
ACE2+/- MC: 5'-AACTTTTCCAGTACTGTAGATGGTGCTCATTGT

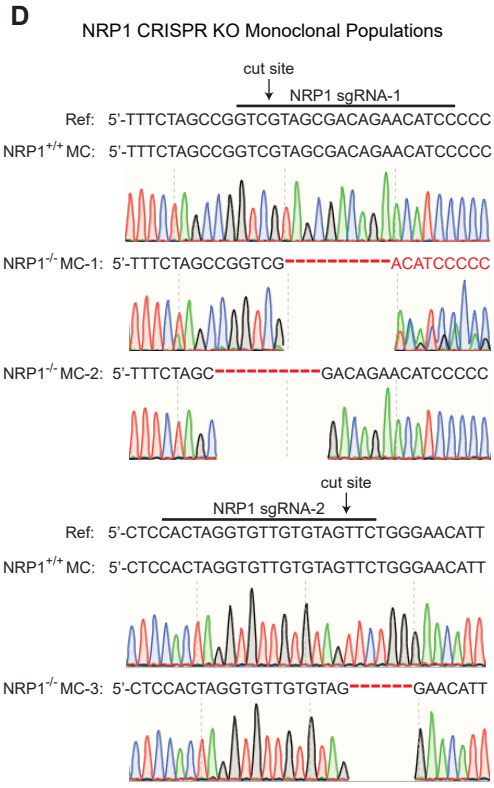
D
NRP1 CRISPR KO Monoclonal Populations
cut site
NRP1 sgRNA-1
Ref: 5'-TTTCTAGCCGGTCGTAGCGACAGAACATCCCCC
NRP1+/+ MC: 5'-TTTCTAGCCGGTCGTAGCGACAGAACATCCCCC
NRP1-/- MC-1: 5'-TTTCTAGCCGGTCG----------ACATCCCCC
NRP1-/- MC-2: 5'-TTTCTAGC----------GACAGAACATCCCCC
cut site
NRP1 sgRNA-2
Ref: 5'-CTCCACTAGGTGTTGTGTAGTTCTGGGAACATT
NRP1+/+ MC: 5'-CTCCACTAGGTGTTGTGTAGTTCTGGGAACATT
NRP1-/- MC-3: 5'-CTCCACTAGGTGTTGTGTAG------GAACATT

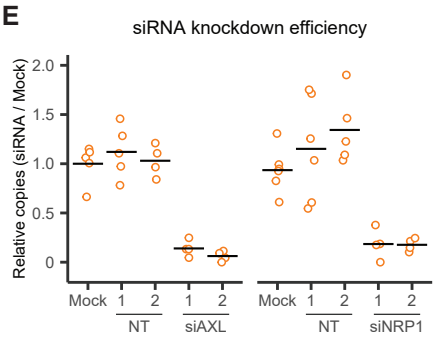
E
siRNA knockdown efficiency
Relative copies (siRNA / Mock)
2.0
1.5
1.0
0.5
0
Mock
1
2
1
2
Mock
1
2
1
2
NT
siAXL
NT
siNRP1

Figure S3

Figure S3. ACE2 and NRP1 knockout via CRISPR in H522 and Calu-3 cell lines, related to Figure 3. A, Genomic Cleavage Detection Assay (Invitrogen) was performed following the manufacturer's protocol on ACE2 WT or ACE2 KO CRISPR modified polyclonal cells. **B**, Sanger sequencing of genomic *ACE2* at exon 3. Unique monoclonal populations of H522 ACE2 KO's were aligned to the human genome ('Ref'; hg38). The red dashed lines indicate small deletions within exon 3 of ACE2. **C**, Monoclonal populations of NRP1 CRISPR cells were infected with SARS-CoV-2 at an MOI: 1 i.u./cell and cell associated vRNA levels quantitated at 4 and 72 hpi (n= 3-6). **D**, Sanger sequencing of genomic *NRP1* at exon 4. Unique monoclonal populations of H522 NRP1 KO's were aligned to the human genome ('Ref'; hg38). The red dashed lines indicate small deletions within exon 4 of NRP1. **E,** NRP1 and AXL siRNA knockdown efficiencies in H522 cells relative to Mock was assessed by Q-RT-PCR 48 h post transfection (n=3-5).

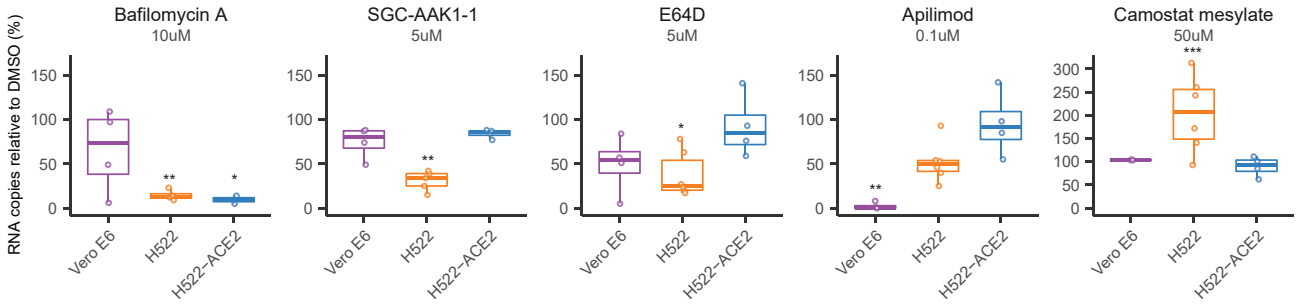
Bafilomycin A
10uM
SGC-AAK1-1
5uM
E64D
5uM
Apilimod
0.1uM
Camostat mesylate
50uM
RNA copies relative to DMSO (%)
Vero E6
H522
H522-ACE2

Figure S4

Figure S4. Comparative analysis of infection pathways in H522 and other permissive cells, related to Figure 4. H522, H522-ACE2 and Vero E6 cells were pre-treated with bafilomycin A (vATPase inhibitor), SGC-AAK1-1 (clathrin-mediated endocytosis inhibitor), E64D (endosomal cathepsins inhibitor), apilimod (PIKfyve inhibitor), or camostat mesylate (TMPRSS2 inhibitor) for 1 h and then infected with SARS-CoV-2 in the presence of the inhibitors. Cell-associated SARS-CoV-2 RNA was detected by qRT-PCR 24 hpi and normalized to DMSO treated cells ($n \geq 3$). * indicates $p<0.05$, ** indicates $p<0.01$, and *** indicates $p<0.001$ compared to DMSO treated controls where significance was determined using two-way ANOVA and the Dunnett correction for multiple comparisons.

ECT2-KIF23-RACGAP1 complex
actomyosin contractile ring assembly
spindle midzone

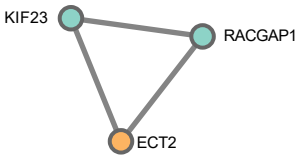

p27-cyclinE-CDK2 complex
G1/S transition of mitotic cell cycle

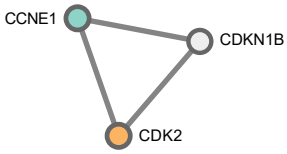

CDC2-CCNA2-CDK2 complex
cell cycle

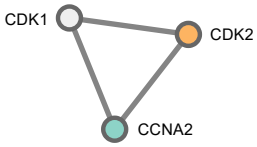

RasGAP-AURKA-survivin complex
mitotic cell cycle
G-protein coupled receptor signaling pathway

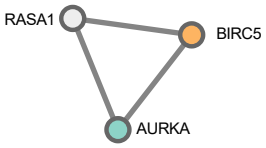

AuroraB-AuroraC-INCENP complex
protein folding and stabilization

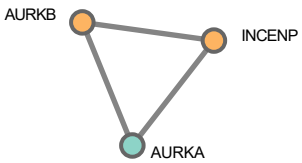

RasGAP-AURKB-survivin complex
mitotic cell cycle
G-protein coupled receptor signaling pathway

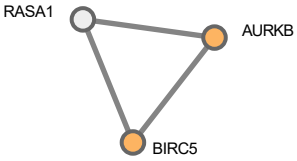

BRIC5-AURKB-INCEN-EVI5 complex
cytokinesis
barrier septum assembly

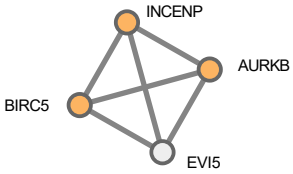

CRM1-Survivin-AuroraB mitotic complex
mitotic cell cycle
nuclear transport

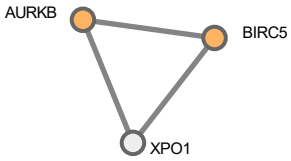

Chromosomal passenger complex
mitotic cell cycle
spindle assembly

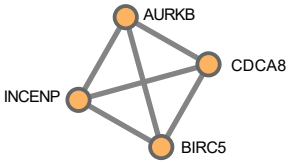

BRCA1-IRIS-pre-replication complex
DNA replication

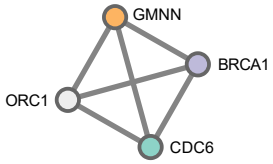

MIS18 complex
centromere complex assembly
regulation of CENP-A containing nucleosome assembly

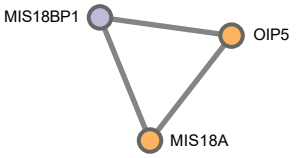

GINS complex
Pre-replicative complex assembly

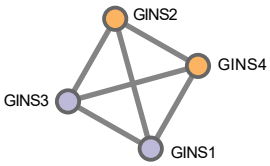

Chromatin assembly complex (CAF-1)
DNA replication
mitotic S phase
chromosome organization

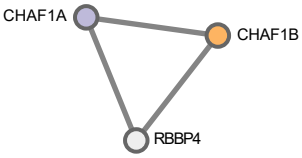

BRD7-EZH2-SUZ12 complex

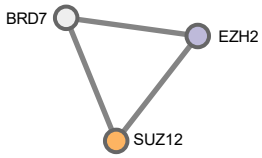

BRCC complex
DNA repair
cell cycle checkpoint
protein ubiquitination

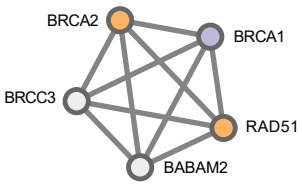

KNL1-MIS12-NDC80-SPC24-ZWINT complex
mitotic cell cycle checkpoint

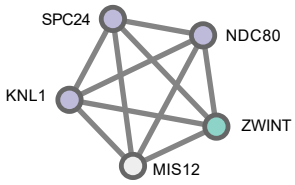

BARD1-BRCA1-CSTF64 complex
RNA 3'-end processing

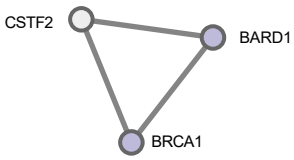

NDC80 kinetochore complex
mitotic cell cycle
chromosome segregation

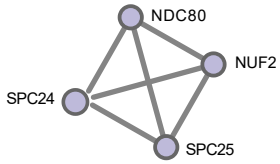

E3 ubiquitin ligase - UbcH5c complex
protein ubiquitination
DNA damage response

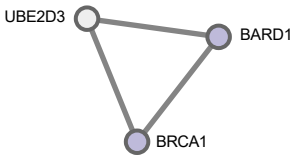

BRCA1 B complex
DNA recombination

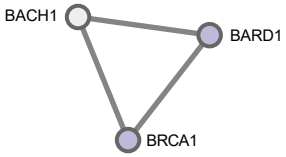

BRCA1-BARD1-POLR2A complex
regulation of RNA biosynthetic process
regulation of transcription

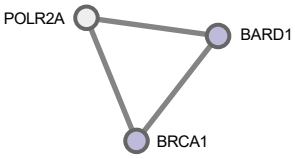

BRAC1-BARD1-UbcH7c complex
DNA damage response

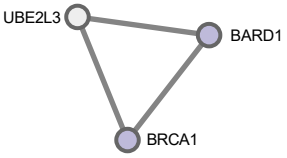

APP-APBB1-LRP1 complex
protein processing (proteolytic)

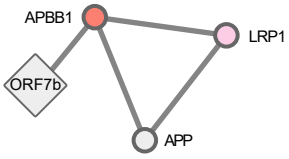

Interferon-stimulated gene factor
transcription complex 3

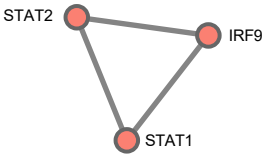

DTX3L-PARP9-STAT1 complex
Defense response to viruses
Protein ubiquitination

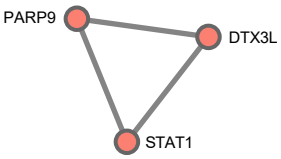

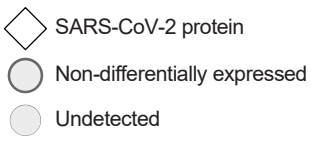

Figure S5

Figure S5. Protein interaction networks of differentially expressed proteins in H522 cells infected with SARS-CoV-2, related to Figure 6. Protein complexes of differentially expressed H522 and SARS-CoV-2 proteins. Complexes and functions were extracted from the CORUM database. The colors correspond to the whole cell proteomic clusters identified in ‘Fig. 6D’.

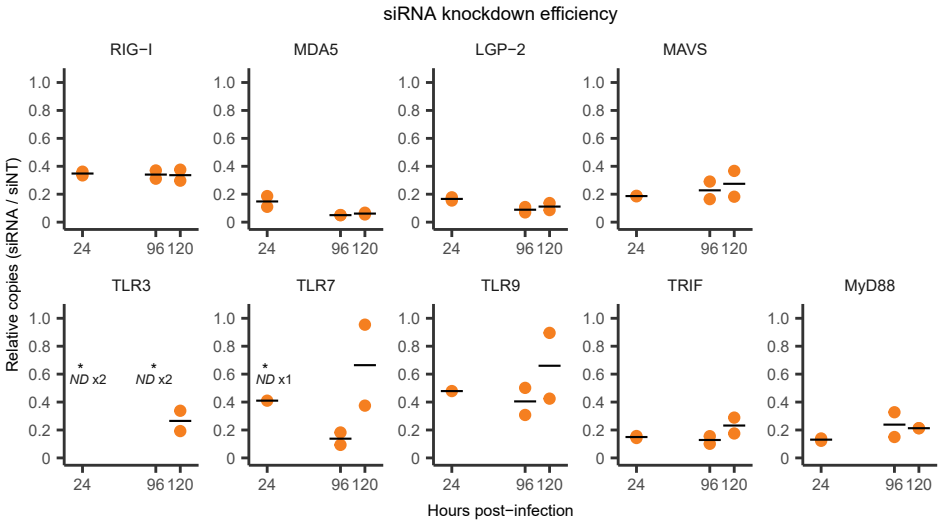
siRNA knockdown efficiency
RIG−I
MDA5
LGP−2
MAVS
TLR3
TLR7
TLR9
TRIF
MyD88
Relative copies (siRNA / siNT)
Hours post−infection
ND x2
ND x2
ND x1
1.0
0.8
0.6
0.4
0.2
0
24
96
120

Figure S6

Figure S6. siRNA knockdown efficiency for viral sensing pathways in H522 cells, related to Figure 7. qRT-PCR for each gene targeted by siRNA in H522 cells. Knockdown efficiency was calculated compared to a non-targeting (NT) control. H522 cells were infected with SARS-CoV-2 24 hpi and RNA was collected 24, 96, and 120 hpi. TLR8 mRNA was not detected across the three time points.